1486 *Biochemistry* **2010,** *49,* 1486–1494
DOI: 10.1021/bi9016523

BIOCHEMISTRY
including biophysical chemistry & molecular biology
Article

Electron Spin-Echo Envelope Modulation (ESEEM) Reveals Water and Phosphate Interactions with the KcsA Potassium Channel[†,‡]

John A. Cieslak, Pamela J. Focia, and Adrian Gross*

Department of Molecular Pharmacology and Biological Chemistry, Northwestern University Feinberg School of Medicine, 303 East Chicago Avenue, Chicago, Illinois 60611

Received September 21, 2009; Revised Manuscript Received January 18, 2010

ABSTRACT: Electron spin-echo envelope modulation (ESEEM) spectroscopy is a well-established technique for the study of naturally occurring paramagnetic metal centers. The technique has been used to study copper complexes, hemes, enzyme mechanisms, micellar water content, and water permeation profiles in membranes, among other applications. In the present study, we combine ESEEM spectroscopy with site-directed spin labeling (SDSL) and X-ray crystallography in order to evaluate the technique's potential as a structural tool to describe the native environment of membrane proteins. Using the KcsA potassium channel as a model system, we demonstrate that deuterium ESEEM can detect water permeation along the lipid-exposed surface of the KcsA outer helix. We further demonstrate that ^{31}P ESEEM is able to identify channel residues that interact with the phosphate headgroup of the lipid bilayer. In combination with X-ray crystallography, the ^{31}P data may be used to define the phosphate interaction surface of the protein. The results presented here establish ESEEM as a highly informative technique for SDSL studies of membrane proteins.

Electron spin-echo envelope modulation (ESEEM)[1] is a pulsed electron paramagnetic resonance (EPR) technique that monitors nuclear magnetic resonance (NMR) transitions indirectly through EPR transitions (*1*). In the experiment, the electron spin-echo amplitude is monitored as it is modulated by the nuclear spin of nearby atoms at characteristic electron−nuclear double resonance (ENDOR) frequencies (*2*). ESEEM has been widely used for the study of paramagnetic metal centers in metalloproteins (*3*−*6*). Typically, ESEEM spectroscopy has been utilized to study metal binding, coordination, radical formation, and metalloenzyme mechanisms. In addition, ESEEM spectroscopy has been used to investigate D_2O permeation profiles in membranes (*7*, *8*) and to study membrane insertion of antimicrobial peptides (*9*, *10*). Recently, ESEEM has also been used to study the major light harvesting membrane protein complex of green plants (LHCIIb) in detergent micelles (*11*).

The technique's requirement of a paramagnetic center can be satisfied by site-directed spin labeling (SDSL) (*12*−*15*). SDSL involves the introduction of a nitroxide at a location of interest in the protein through molecular engineering (Figure 1A). SDSL has been used to probe structure in a variety of membrane protein systems, including bacteriorhodopsin, rhodopsin, porins, and potassium channels (*12*−*15*). Most applications of SDSL have utilized continuous wave (CW) EPR techniques and include nitroxide scanning applications with the goal of determining the underlying secondary structure of a sequence of interest, the measurement of molecular distance distributions between pairs of nitroxides, and the detection of conformational changes during function. In addition, CW-EPR can provide a measure of polarity surrounding the nitroxide side chain (*16*, *17*). The polarity effects are mediated through the degree and direction of hydrogen bonding of the nitroxide with the nearby environment and are measured by determining the **A** and **g** tensor elements of the nitroxide (*18*). However, the identity of the hydrogen-bonding partner of the nitroxide typically remains unknown.

Alternatively, the polarity and accessibility of the nitroxide environment can be determined using collision studies (*19*, *20*). In membrane proteins, these experiments typically involve exposing labeled and reconstituted protein with hydrophilic (NiEDDA) and hydrophobic (oxygen) paramagnetic colliders that provide additional T_1 relaxation pathways to the nitroxide thorough Heisenberg spin exchange. These collision studies are limited by the fact that spin exchange requires direct physical contact between the nitroxide and the paramagnetic collider with a collision radius equal to the sum of the effective radii of the two species (*20*). In contrast, ESEEM is based on through-space anisotropic hyperfine interactions between the nitroxide and nearby nuclear spins. The amplitude of the ESEEM signal depends on both the number of nearby nuclei (N) and the

[†]This work was supported by NIH Grant GM58568 to A.G. and NIH Fellowship NS051095 to J.C.

[‡]The coordinates and structure factors of KcsA-V48R1 have been deposited with the Protein Data Bank (accession code 3IFX).

*To whom correspondence should be addressed. Telephone: (312) 503-3375. Fax: (312) 503-5349. E-mail: a-gross@northwestern.edu.

[1]Abbreviations: CW, continuous wave; DOXYL, 4,4-dimethyloxazolidine-*N*-oxyl; DPPC, dipalmitoylphosphatidylcholine; ENDOR, electron−nuclear double resonance, EPR, electron paramagnetic resonance; ESEEM, electron spin-echo envelope modulation; Fab, fragment−antigen binding; HYSCORE, hyperfine sublevel correlation; IPTG, isopropyl β-D-1-thiogalactopyranoside; KCl, potassium chloride; MHz, megahertz; MTSL, *S*-(2,2,5,5-tetramethyl-2,5-dihydro-1*H*-pyrrol-3-yl)methyl methanesulfonothioate; NiEDDA, nickel(II) ethylenediaminediacetate; NMR, nuclear magnetic resonance; POPC, 1-palmitoyl-2-oleoyl-*sn*-glycero-3-phosphocholine; POPG, 1-palmitoyl-2-oleoyl-*sn*-glycero-3-[phospho-*rac*-(1-glycerol)]; R1, designation for spin-labeled side chain; SDSL, side-directed spin labeling; TEMPO-PC, 1-palmitoyloleoyl-*sn*-glycero-3-phospho(4-[*N*,*N*-dimethyl-*N*-(2-hydroxyethyl)]ammonium-2,2,6,6-tetramethylpiperidine-1-oxyl)choline; TM, transmembrane segment; Tris, tris(hydroxymethyl)aminomethane; T1, electron spin−lattice relaxation time.

 Published on Web 01/21/2010

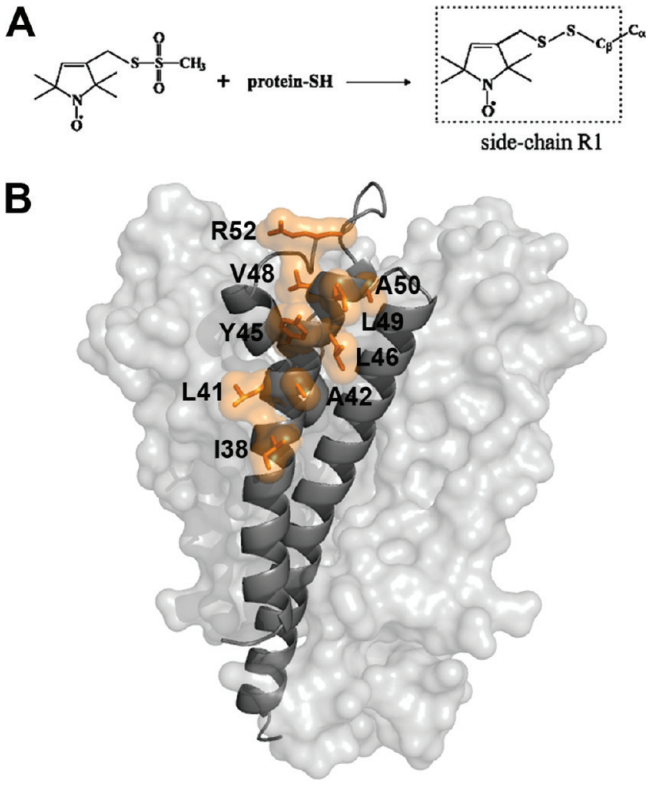

FIGURE 1: Site-directed spin labeling of KcsA. (A) Reaction of the methanethiosulfonate reagent with cysteine to generate the side chain designated R1. (B) Labeled sites in KcsA. A KcsA monomer is shown as a gray ribbon with the rest of the channel depicted as a van der Waals surface. The side chains of labeled sites are depicted as orange sticks and van der Waals surfaces.

distance between nuclear and electron spins (R) and is proportional to N/R^6. For instance, a deuterium nucleus can be detected at a distance of up to 6−8 Å (*9*). ESEEM, therefore, can determine the atomic environment surrounding a nitroxide without direct physical contact with the interacting species.

In the present study, we applied ESEEM in combination with SDSL in order to determine the native environment of a membrane protein of known structure reconstituted in lipid vesicles. The KcsA potassium channel is well suited for these studies because it is easily overexpressed in *Escherichia coli*, is well-behaved biochemically, and can be functionally reconstituted in lipid vesicles (*21*, *22*). In addition, the structure of KcsA is known to high resolution (*23*), and extensive biophysical studies support the notion that the crystal structure represents the predominant native state of the channel (*24*−*26*). Specifically, we determined the water permeation profile along the surface of the outer transmembrane helix of KcsA using D_2O as a water substitute and deuterium substrate. We found that deuterium interactions with the outer helix decrease with increasing immersion depth into the membrane. This decrease of water permeation was similar compared with empty lipid vesicles of the same composition. In addition, we identified two KcsA residues that are within interaction distance to the phosphate headgroup of the membrane, as determined through ^{31}P-nitroxide coupling. The crystal structure of one of these two constructs allows the determination of the phospholipid headgroup interaction surface of the channel. The data suggest that ESEEM is well suited for structural studies of membrane proteins and can provide key insight into their local native environment.

MATERIALS AND METHODS

Protein Expression, Purification, Labeling, and Reconstitution. KcsA was overexpressed, purified, and spin-labeled as previously described (*26*−*28*). Labeled KcsA was further purified by gel filtration on Superdex 200 in a buffer containing 20 mM Tris, pH 8.0, 150 mM KCl, and 5 mM decyl maltoside and reconstituted on Sephadex G-50 (both GE Healthcare) into 4:1 1-palmitoyl-2-oleoyl-*sn*-glycero-3-phosphocholine (POPC)−1-palmitoyl-2-oleoyl-*sn*-glycero-3-[phospho-*rac*-(1-glycerol)] (POPG) liposomes (Avanti Polar) at a molar lipid:protein ratio of ~1000:1 by the method of Green and Bell (*29*). Proteoliposomes were pelleted by centrifugation (20 h at 400000*g*) and resuspended to a KcsA concentration of ~200 μM with a solution of 50 mM Tris, pD 7.4, 150 mM KCl, and 25% glycerol for cryoprotection. The samples were flash frozen in liquid nitrogen and stored at −80 °C until measurement.

Preparation of Doped Empty Vesicles. 1-Palmitoyl-2-stearoyl-(*n*-DOXYL)-*sn*-glycero-3-phosphocholine and 1-palmitoyl-oleoyl-*sn*-glycero-3-phospho(TEMPO)choline (Avanti Polar) were reconstituted on Sephadex G-50 (GE Healthcare) into 4:1 POPC−POPG liposomes (Avanti Polar) at a molar lipid:spin-labeled lipid ratio of ~1000:1 as described above.

EPR Measurements. CW-EPR spectra were recorded at room temperature on an X-band EMX spectrometer fitted with an ER4119HS resonator (Bruker Biospin) at a scan width of 200 G. ESEEM samples were flash-cooled in liquid nitrogen, and the data were recorded at 80 K on an X-band Elexsys-E580 spectrometer fitted with an ER4118X-MS2 resonator (Bruker Biospin). ESEEM data were acquired using a three-pulse sequence ($\pi/2-\tau-\pi/2-T-\pi/2-\tau-$echo) with 16 ns $\pi/2$ pulses at a frequency corresponding to the center line of the nitroxide spectrum. A four-step phase cycle was used to suppress unwanted echoes. Timing parameters were adjusted to obtain optimal modulation by specific nuclei: τ = 224 ns for ^{2}H experiments, τ = 252 ns for ^{31}P experiments, and τ = 128 ns for ^{1}H blind experiments. The time-dependent echo amplitudes are shown in Supporting Information Figure S1 and were processed as described (*7*, *10*). The data were normalized by division through a polynomial fit to the underlying T_1 echo decay, followed by subtraction of unity. The missing data points were obtained by back-prediction using the LPSVD algorithm (*30*). The data were further processed by Hamming apodization, zero filling, and Fourier transformation to obtain frequency domain power spectra with spectral densities with dimension of time (*10*). Three-pulse ESEEM data were simulated (*1*) with different **A** and **g** tensor elements (*31*, *32*) and a single ^{2}H nucleus at 3.2 Å in order to estimate effects due to polarity and nitroxide structure. The error in measurement (< 4%) and effects due to polarity and nitroxide structure (< 1%) were small in relation to the overall variability between protein samples from different expression batches (< 10%). HYSCORE data were acquired using a four-pulse sequence ($\pi/2-\tau-\pi/2-t_1-\pi-t_2-\pi/2-\tau-$echo) with 16 ns $\pi/2$ pulses and a 32 ns π pulse. A four-step phase cycle was used to suppress unwanted echoes. The time-dependent echo amplitudes were processed as described above (without back-prediction), followed by 2D Fourier transformation.

RESULTS

Spin Labeling of the KcsA Outer Helix. Based on the crystal structure of KcsA (*23*), nine residues (I38, L41, A42, Y45,

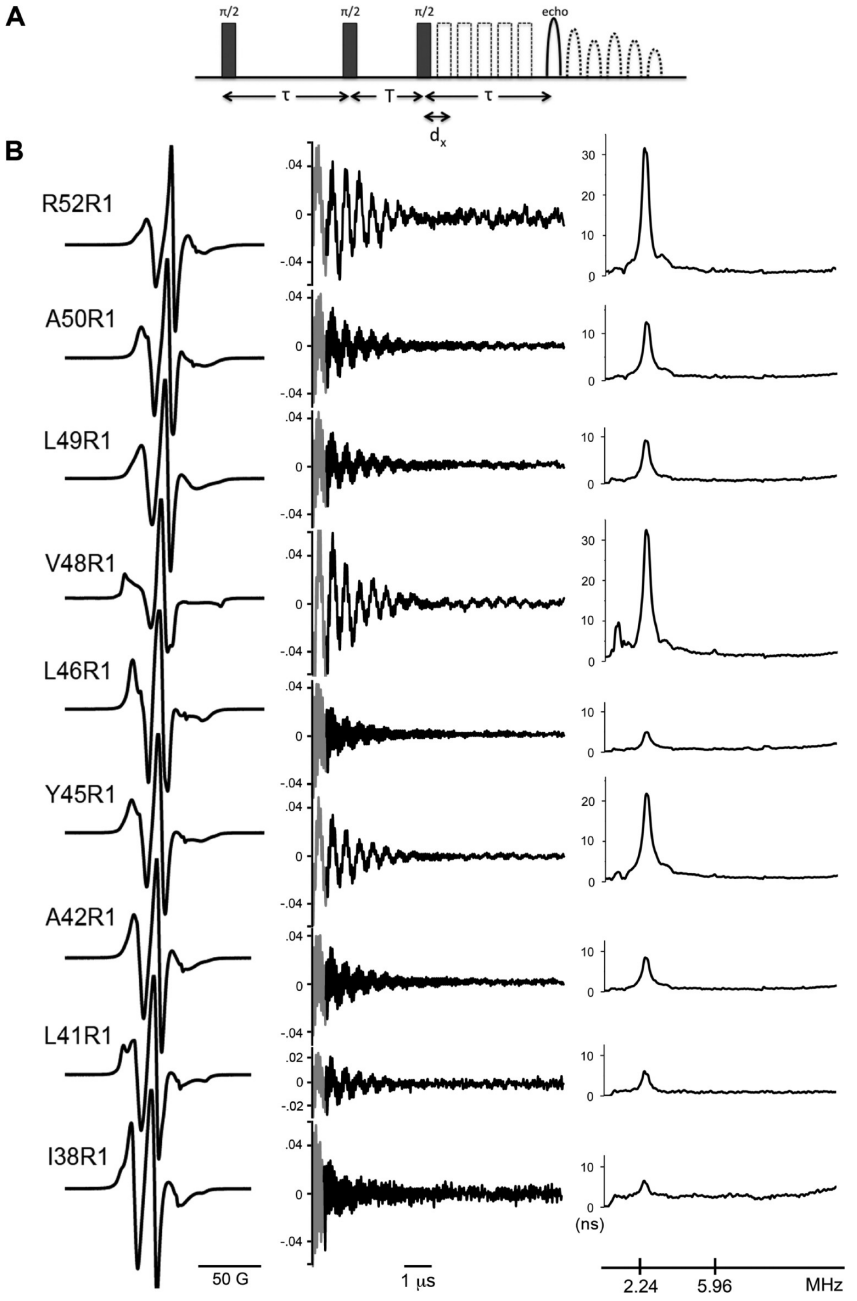

FIGURE 2: Line-shape and ^{2}H ESEEM data of R1 constructs reconstituted in POPC−POPG vesicles. (A) Schematic of the three-pulse ESEEM experimental design. Three $\pi/2$ pulses are separated by the time constants τ and T, with T sequentially delayed by d_x increments, resulting in the modulation of the observed spin echo. The time constant τ is adjusted to tune the system for optimal detection of a frequency of interest. (B) Left: X-band first-derivative absorption spectra acquired at room temperature over a scan width of 200 G. Middle: ESEEM data obtained with $\tau = 224$ ns (to optimize detection of ^{2}H) in the presence of D_2O. The black trace is the normalized time domain data. The gray segment is the back-calculated dead-time signal (see Materials and Methods). Right: Frequency domain ESEEM signal. The deuteron (2.24) and phosphorus (5.96) frequencies are indicated in MHz units.

L46, V48, L49, A50, and R52) were selected along the outer surface of the outer transmembrane helix (Figure 1B). These residues were chosen because they have minimal tertiary interactions with other portions of the protein and are predominately exposed to the outside environment. In addition, all residues are located on the extracellular half of the channel where the structure is known to remain constant independent of the gating state of the channel (*33*). The inner transmembrane helix was avoided due to incomplete labeling along the region of interest (*26*, *33*). The positions of the nine residues range from a lipid-exposed helix surface site in the middle of the membrane (I38) to a solvent-exposed loop site located just above the outer helix (R52). Each residue was mutated to cysteine, and the introduced thiol was reacted with a nitroxide spin label to form the nitroxide side chain denoted R1 (Figure 1A). The labeled mutant channel was then reconstituted in POPC−POPG lipid vesicles by gel filtration (see Materials and Methods). The room temperature CW-EPR spectra at X-band of the selected constructs are shown in Figure 2B. The line shapes of all nitroxides (except V48R1) are indicative of sites with high side chain mobility and are thus consistent with their external position along the outer helix. In contrast, the line shape of V48R1 is indicative of an immobilized nitroxide. The crystal structure of KcsA indicates that the immobilization of the R1 side chain at this position probably

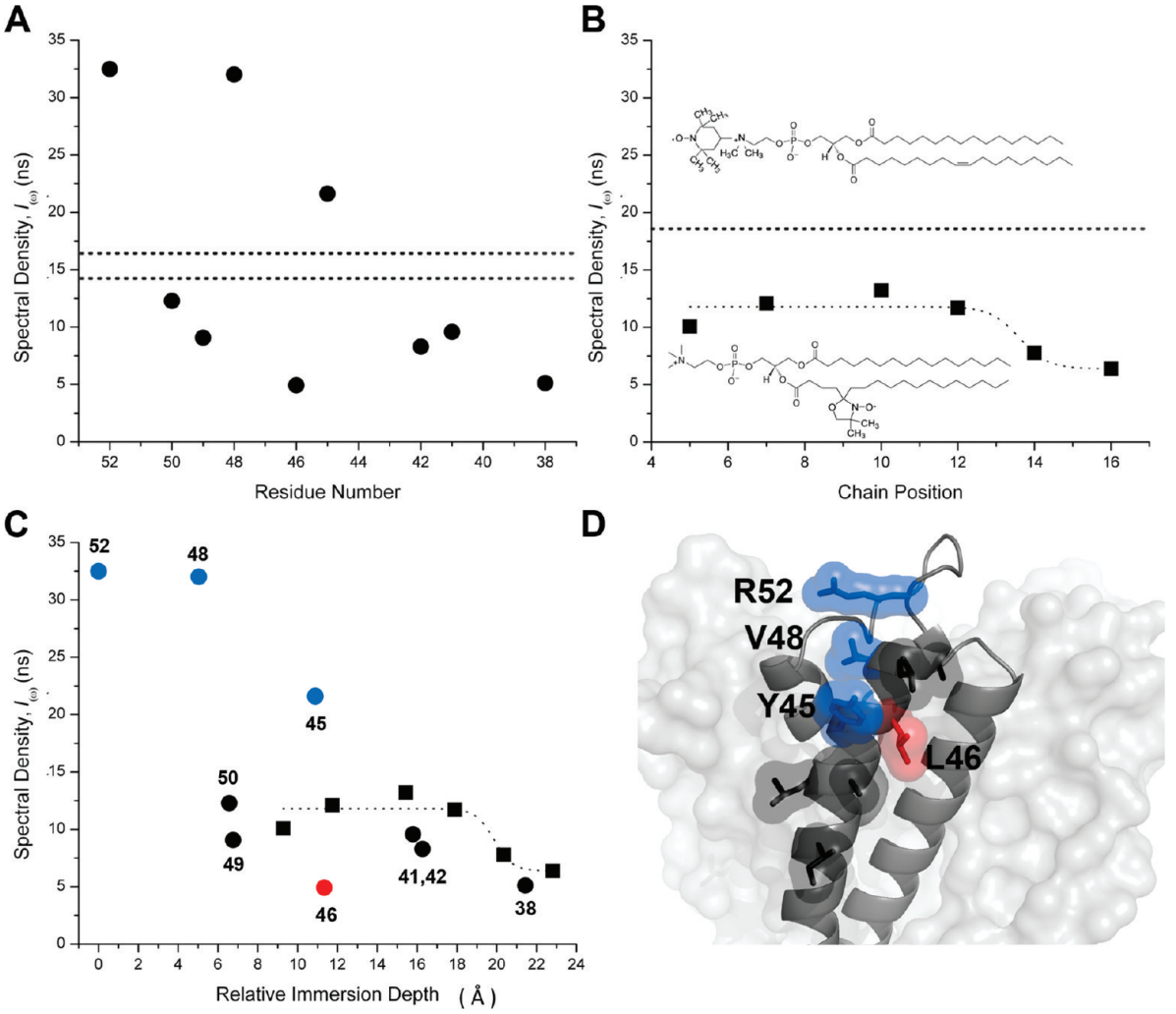

FIGURE 3: KcsA insertion into the membrane preserves the expected water permeation profile. (A) The deuteron spectral density of labeled residues is shown as a function of residue number. Deuterium modulation of the C-terminal mutants F148R1 and L151R1 is represented by the horizontal dashed lines (~14.8 and 16.6 ns, respectively). (B) The deuteron spectral density of spin-labeled lipids in POPC−POPG vesicles plotted as a function of chain position. The dotted line is drawn to support the eye. The dashed line is the deuteron spectral density of TEMPO-PC. Top insert: Structure of TEMPO-PC. Bottom insert: Structure of 5-doxyl-PC. (C) The labeled lipid (squares) and KcsA (circles) deuteron spectral density data superimposed as a function of relative immersion depth (in Å relative to the Cβ position of R52R1). Data for residues Y45R1, V48R1, and R52R1 are colored blue, and L46R1 is colored red. (D) Structural representation of one KcsA subunit depicted as a gray ribbon and the rest of the channel as a van der Waals surface. The studied side chains are depicted in stick representation with accompanying van der Waals surfaces and are colored as in (C).

occurs due to a tertiary contact interaction of the nitroxide with the pore helix of the channel (*23*). The spectra reported here are thus highly consistent with the known structure of KcsA. Furthermore, the spectra are in agreement with results from earlier studies (*25*, *27*).

Deuterium ESEEM Demonstrates Water Permeation along the Hydrophobic Surface of KcsA. The KcsA constructs were analyzed using the three-pulse ESEEM sequence shown in Figure 2A. D_2O was added to the sample in order to isotope label hydrogen derived from water and distinguish it from hydrogen derived from protein and lipid. Figure 2B summarizes the line-shape (left panel) and ESEEM data in both time (middle panel) and frequency domain (right panel) for all sites studied. Proton and deuteron ENDOR frequencies predominate in the ESEEM spectra at all sites. Because the total proton pool in the system arises from multiple sources (protein, lipid, and residual H_2O), the proton spectral density at 14.6 MHz cannot unambiguously be assigned to any one source and was not further analyzed. Figure 3A illustrates the amplitude of the deuteron spectral density at 2.2 MHz as a function of residue position using data from all sites studied. The data indicate that although the absolute deuteron spectral density fluctuates significantly along the transmembrane helix, there is a sizable overall decrease from ~33 ns near the outside surface (R52R1) to ~5 ns near the middle of the membrane (I38R1). In order to place these values into a more meaningful framework, we determined the spectral density at different immersion depths using empty vesicles of the same composition (Figure 3B) doped with trace amounts of spin-labeled phospholipids (lower insert). In these empty vesicles, the deuteron spectral density decreased with an approximately sigmoidal dependence from ~12 to ~6 ns as the spin label was moved along the alkyl chain toward the center of the membrane (*7*).

The deuterium modulation was also measured at the level of the lipid headgroup by means of TEMPO-PC (Figure 3B, upper insert). The spectral density for this interfacial spin label was ~18 ns (dotted line) and thus significantly higher than at any position along the alkyl chain. Simulation studies show that the

different structures of the nitroxide moieties have a negligible impact on the ^{2}H ESEEM data in the current experimental context (data not shown). The data on the empty vesicles are nicely self-consistent and indicate that we can expect decreasing deuteron spectral density as a function of immersion depth, with absolute values ranging from ~18 ns at the water−lipid interface to ~6 ns near the middle of the membrane. We next sought to determine the spectral density of sites on KcsA exposed to bulk water. Two sites known to be located far from the membrane were chosen that had both exhibited exceptionally high NiEDDA accessibility in earlier studies. The side chains of F148R1 and L151R1 are located on the water-exposed C-terminal domain of KcsA and were shown to have the highest NiEDDA accessibility of any residues in that region of the protein (*34*). Interestingly, the deuteron spectral density of these two sites (~14.5 and ~16.5 ns, dotted lines in Figure 3A) is closer to TEMPO-PC (~18 ns) than to R52R1 (~33 ns). It thus appears that the ^{2}H spectral density of V48R1 and R52R1 is exceptionally high.

It is useful for the direct comparison between lipid and protein data to place all spin labels on approximately the same length scale with regard to immersion depth. For the purposes of this study, the immersion depth of KcsA spin labels was defined as the distance (in the direction normal to the membrane surface) between the Cβ of the residue in question and the Cβ of residue R52. R52 is arbitrarily used as a reference point for zero immersion depth in order to generate only positive values. The immersion depth of lipid spin labels is obtained by modeling the doxyl moiety (Figure 3B, lower inset) onto a well-resolved lipid chain observed in the high-resolution structure of KcsA (*23*) and determining the vertical distance component of the spin label with respect to R52. The resulting graph (Figure 3C) demonstrates an overall similar depth dependence at some KcsA sites compared to the lipid data. The new depth scale has eliminated some of the original data scatter, and the only remaining significant outliers are the lower than expected ^{2}H spectral density for residue L46R1 (red), located at an immersion depth of ~11 Å, and the higher than expected ^{2}H spectral densities for Y45R1, V48R1, and R52R1 (blue). What is apparent in the data is that the insertion of KcsA into the membrane did not lead to generally increased water permeation along the surface of the protein when compared to empty vesicles. To the contrary, the lower than expected ^{2}H spectral density of residue L46R1 indicates less water permeation in the vicinity of this residue than at comparable depths in empty vesicles.

^{31}P ESEEM Identifies Residues Interacting with the Phosphate of the Membrane. The frequency domain spectra at superficially located sites, in particular V48R1 and R52R1, show hints of weak ^{31}P modulation near 6.0 MHz that is absent in more lipid-immersed sites (Figure 2B). ^{31}P is the only nucleus in the system that can account for interactions at this frequency. In order to further confirm the interaction at these two positions, the ESEEM experiment was repeated with a pulse sequence tuned to optimize detection of ^{31}P (Figure 4A). The data confirm ^{31}P modulation near the detection limit, corresponding to a ^{31}P−nitroxide spin−spin distance of ~5 Å (*35*). The van der Waals surfaces occupied by the two ^{31}P-modulated nonaromatic residues are contiguous and are located above a ring of membrane-exposed aromatic residues in KcsA (Figure 4B), consistent with an interaction between the two side chains and the surrounding phosphate headgroup layer of the membrane. In addition, one of the interacting residues is R52; arginines are well-known to interact closely with the phosphate moiety of

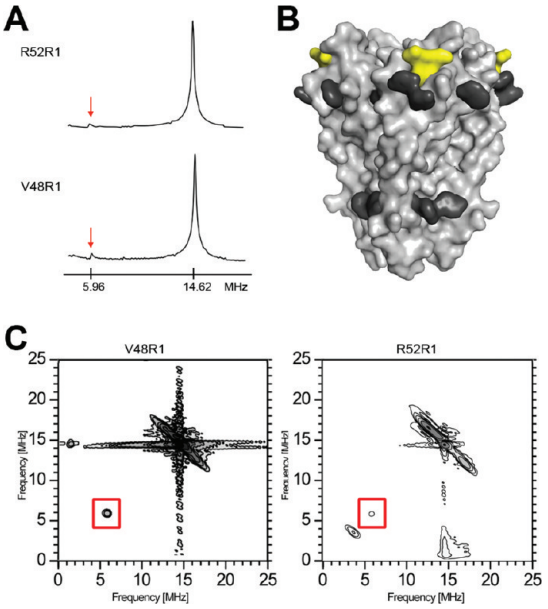

FIGURE 4: ^{31}P ESEEM of reconstituted KcsA. (A) Frequency domain ESEEM spectra of the KcsA constructs V48R1 and R52R1 using a time constant optimized for ^{31}P modulation (τ = 252 ns). The phosphorus (5.96 MHz) and proton (14.62 MHz) Larmor frequencies are indicated. (B) The phosphorus interaction surface of KcsA is depicted as a yellow van der Waals surface. The side chains of aromatic residues believed to be exposed toward the water−lipid interface are highlighted in dark gray (*38*). (C) Frequency domain HYSCORE spectra of V48R1 (optimal time constant to observe ^{31}P modulation, τ = 252 ns) and R52R1 (optimal time constant to suppress ^{1}H modulation, τ = 128 ns). The phosphorus Larmor frequency peak at 5.96 MHz is boxed.

membranes (*36*). The ^{31}P modulation at residues V48 and R52 was further confirmed by a 2D-HYSCORE experiment (Figure 4C) (*37*). In order to minimize deuteron interference and to clarify the spectra, the HYSCORE samples were prepared in a buffer without added D_2O. As expected, both V48R1 and R52R1 spectra show the required diagonal peaks corresponding to ^{1}H and ^{31}P (14.6 and 6.0 MHz, respectively). The off-diagonal splitting of the ^{1}H peak is probably due to interactions of the unpaired electron with nearby protons on the nitroxide ring or with hydrogen-bonded water.

If the precise position of the two nitroxides were known, then the observed ^{31}P spectral densities could be used to approximately determine the position of the interacting phospholipid headgroup. Given the highly immobile CW-EPR spectrum of residue V48R1 (Figure 2B), it appeared feasible to crystallographically resolve the R1 side chain in this construct. Unfortunately, high-quality KcsA−Fab cocrystals could not be grown due to steric interference of the labeled residue with Fab binding (data not shown). Nevertheless, data to an effective resolution of 3.5 Å Bragg spacings were obtained in the absence of a Fab fragment using the original crystallization protocol of the isolated channel (*38*) (Supporting Information Table S1). Figure 5A shows that the observed electron density for V48R1 clearly determines the position of the R1 side chain.

If it is assumed that the phosphorus modulation at both sites originates from the same ^{31}P nucleus, a reasonable assumption given the relative scarcity of phosphorus in the system under study, then this nucleus must be located at the intersection of the surfaces of two spheres with radius 5 Å, centered at the position of the two nitroxide spins (Figure 5B). However, unlike V48R1, the highly mobile CW-EPR spectrum of R52R1 (Figure 2B)

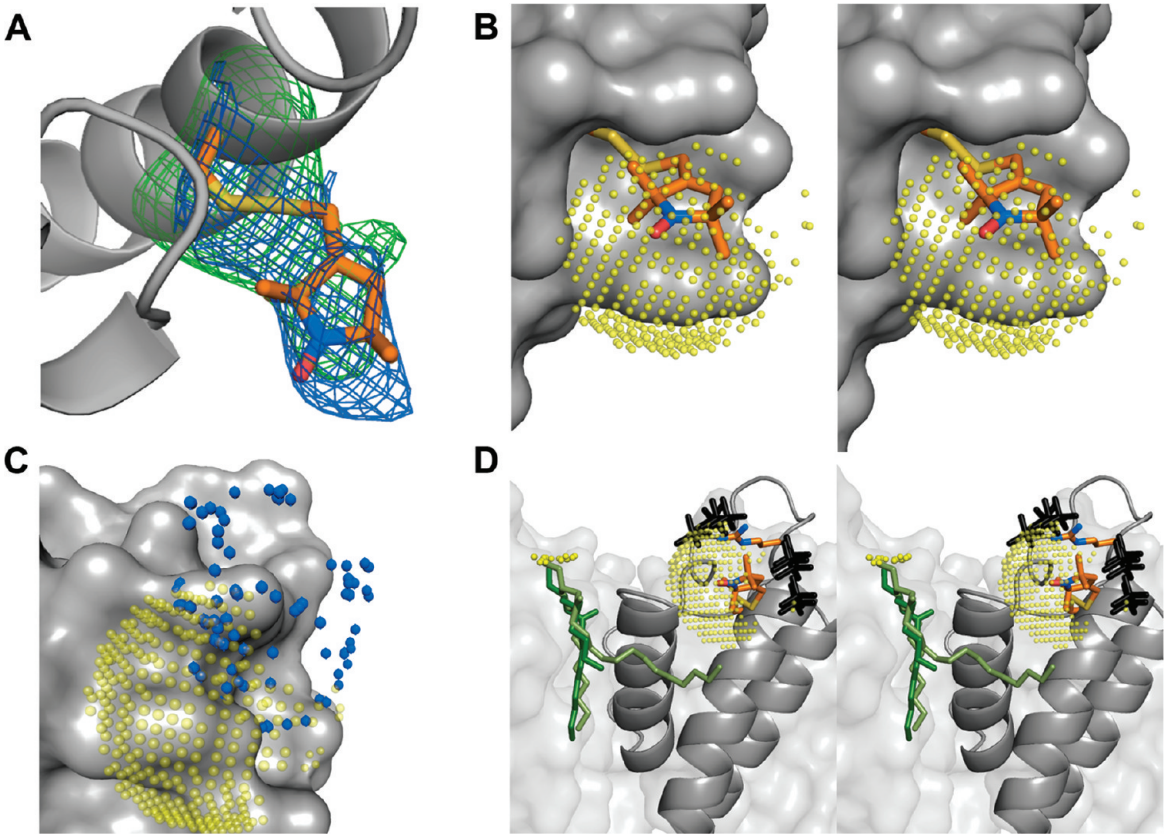

FIGURE 5: The structure of V48R1 and the phosphate interaction surface. (A) KcsA is shown as a gray ribbon, and the V48R1 side chain is shown in stick representation with carbon, nitrogen, oxygen, and sulfur atoms colored orange, blue, red, and yellow, respectively. The $2F_o - F_c$ map is contoured at 1σ (blue), and the $F_o - F_c$ map is contoured at 2.7σ (green). (B) Stereoview of V48R1 with a 5 Å ^{31}P ESEEM interaction surface (yellow spheres) centered on the nitroxide nitrogen. The sphere is sampled at ~0.5 Å, and only sterically feasible areas of the sphere are shown. KcsA is shown as a gray van der Waals surface. (C) Possible positions of the R52R1 nitroxide nitrogen based on preferred nitroxide dihedral angles (*39*) are shown as blue spheres together with the KcsA channel as a gray van der Waals surface and the yellow V48R1 interaction surface. (D) Stereoview of sterically feasible phosphate positions (black) assuming the presence of a R52−phosphate interaction located on the V48R1 interaction surface (yellow); i.e., both V48R1 and R52R1 couple to the same phospholipid. The side chains of R52 and V48R1 as well as a crystallographically observed lipid (two alternative green models, see PDB entries 1K4C and 1R3J) are shown in stick representation. The position of the phosphate headgroup of the lipid is not resolved. Possible positions of the phosphorus are shown as small yellow spheres.

indicates the presence of a highly disordered side chain, meaning that a crystal structure of this construct is unlikely to provide a defined position of the nitroxide moiety. Although the position of the unpaired electron at this site cannot be determined precisely, the accessible volume of the side chain can be obtained based on the structure of R1 and the knowledge of its preferred dihedral angles (Figure 5C) (*39*). If we assume that the R52 side chain closely interacts with the phosphate under native conditions, then the known preferred dihedral angles of arginine, the possible volume of the R52R1 side chain, the position of the V48R1 spin, and the size and geometry of phosphate jointly constrain the possible position of the phosphate headgroup (Figure 5D).

DISCUSSION

Deuterium ESEEM. In contrast to the established collision-based EPR techniques for determining membrane exposure (*19*, *40*), ESEEM does not require direct physical access of a collider to the R1 side chain. Physical access of a collider places limits on the types of environments that can be studied by the CW-EPR methodology. This limitation was demonstrated for sites in the internal water-filled cavity of KcsA, which were found to be essentially inaccessible to NiEDDA even though they were located in an aqueous environment (*26*). The ESEEM approach described here overcomes this limitation by directly determining the deuterium environment surrounding the spin label, independent of any other access parameters. As expected, the two measurements are highly correlated for the structurally unconstrained and solvent-exposed residues studied here (Supporting Information Figure S2). The manner in which deuterium is introduced allows for some future technique development. It is conceivable, for instance, that the deuterium can be introduced selectively, such as at limited positions on the alkyl chain of lipids (*41*) or at specific amino acids on the channel (*42*). Indeed, studies with spin-labeled peptide inserted into deuterated lipid vesicles have been performed (*9*, *43*). In the present study, deuterium was introduced nonselectively in the form of D_2O. Deuterium nuclei are thus present either as part of water or as part of protein or lipid through the mechanism of proton−deuteron exchange. Since proton−deuteron exchange requires D_2O access to the site, it is unnecessary to be able to separate the two sources of deuterons for the purposes of this study. The penetration of water into the membrane is followed through the amplitude of deuterium modulation. The amplitude of the deuterium modulation of the electron spin is dependent on both the distance between the interacting nuclei and the spin (R), as well as the number of interacting nuclei (N), and is proportional to N/R^6. The high order dependence on distance and the magnetic properties of deuterium ensure that only nuclei within

~6−8 Å can contribute to the deuterium signal (*9*). Furthermore, the modulation is weighted heavily in favor of the closest interacting nuclei. Therefore, water permeation profiles determined by ESEEM are correlated to the local concentration of D_2O and strongly weighted by the deuteron−spin distance distribution. The high order dependence on distance means that different rotameric distributions of R1 along the TM1 helix may affect the measured deuteron spectral density. While side chains that are immobilized (V48R1) at room temperature are expected to also occupy a single rotamer at low temperature, more mobile side chains (I38R1, L49R1) sample multiple rotamers at room temperature and are likely to freeze into rotamer distributions with distinct deuterium environments. It is therefore to be expected that, in the limit, highly ordered water surrounding a highly ordered spin label could give rise to exceptionally high spectral densities. The technique may thus be more robust when highly mobile nitroxides are studied as they sample a large volume of space, in effect averaging out the local D_2O distribution experienced by any one rotameric state.

Water Permeation in Empty Vesicles. It has previously been shown that water permeation into saturated DPPC vesicles can be determined by deuterium ESEEM and that the permeation profile has a sigmoidal, trough-like form (*7*). The permeation profile of unsaturated POPC−POPG vesicles determined here (Figure 3B) shows a similar overall form, but the point of maximal gradient is shifted toward deeper positions. In POPC−POPG membranes the gradient is highest at approximately chain position 13, whereas the equivalent point occurs at chain position 11.6 in unsaturated DPPC vesicles (*7*). The higher water penetration into membranes comprised of unsaturated lipids is expected and can be explained by the increased interlipid packing distance that exists due to unsaturation. The transition from high water permeation near the outer surface of the lipid bilayer to low water permeation in the middle of the membrane is also affected by temperature. In frozen membranes, the transition point is shifted to slightly deeper chain positions than are observed in fluid membranes (*16*). Nevertheless, the structure and biophysical properties of membranes are well preserved upon freezing under cryoprotecting conditions (*7*, *8*, *35*, *44*).

Water Permeation along the Surface of the Outer Helix. When an integral membrane protein is inserted into a membrane, a boundary layer of lipids is generated that may have an altered water permeation profile than the more distant parts of the membrane. In the case of KcsA, however, the water permeability along the protein surface does not appear to increase over the level observed in empty vesicles (except for Y45R1, which is located at the water−lipid interface). Therefore, KcsA does not introduce water-accessible crevices along its surface. To the contrary, part of the protein surface may be exposed to less water than would be expected in empty vesicles. Specifically, sites L41R1, A42R1, and L46R1 show lower apparent water penetration than would be expected based on their relative immersion depths. Interestingly, the lowest ^2H spectral density is observed for a residue (L46R1) that projects into a groove between two transmembrane helices (Figure 3D). KcsA is known to order lipids in grooves between transmembrane helices (Figure 5D) (*23*) leading to locally dry protein surface areas. Alternatively, or in addition, a slight bend of the outer helix increases the effective immersion depth of this residue with respect to the other sites studied (Figure 3D). The very low water permeation at site L46R1 is also supported by NiEDDA accessibility data that show a lower than expected accessibility at this site (*25*).

It remains unclear why the deuterium modulation is so high for V48R1 and R52R1. As we did not exhaustively search for high deuterium modulation, it remains possible that other residues exposed to bulk water could show similarly high deuteron spectral densities. We selected the two specific residues on the C-terminal of KcsA because we reasoned that residues exhibiting exceptionally high NiEDDA collision rates were good candidates to reflect the expected deuterium modulation of a highly water-exposed nitroxide. If this reasoning is sound, then the deuterium modulation of V48R1 and R52R1 is indeed exceptionally high. It is noteworthy that the two nitroxides show very different side chain mobilities at room temperature, arguing against locally ordered water located very close to the side chain as the reason for the high spectral density. Further studies are required to determine whether these densities are indeed exceptional and whether these high values are related to the other aspect that distinguishes these two residues, namely, their close interaction with the phosphate headgroup of a nearby lipid.

Phosphorus ESEEM. Unlike deuteron and proton, ^{31}P is a rare nucleus in the experimental system under study. The only natural source of phosphorus is the phosphate headgroup of the membrane in which the channel is reconstituted. Based on the geometry of phospholipid packing in membranes, approximately one ^{31}P nucleus is expected per 50 $Å^2$ of membrane surface (*45*). The modulation depth of the ^{31}P nucleus is smaller than that of ^2H (*46*). As a consequence, the presence of a ^{31}P nucleus can only be detected to a distance of ~5 Å from the nitroxide, whereas a single ^2H nucleus can interact up to 6−8 Å (*9*, *35*, *46*). Because of the overall scarcity and regular occurrence of phosphorus, it is reasonable to treat phosphorus modulations as if they originated from a single nucleus. The high order dependence on distance and the nuclear properties of ^{31}P limit the number of residues with observable modulation and allow an accurate map of the phosphate interaction surface of KcsA to be made (Figure 4B). The accuracy of the map is further improved if the precise position of the nitroxide side chain can be determined through X-ray crystallography (Figure 5D).

Locating the Interacting Phosphate Headgroup. The magnitude of the magnetic interaction determined by ESEEM is dominated by the closest distance between the nucleus and nitroxide spin. Accordingly, the interaction can be analyzed assuming a single nucleus approximation in order to obtain a lower bound value for the distance of interaction (*47*). Applying these principles, we conclude that the interacting ^{31}P nucleus is located ~5 Å from both V48R1 and R52R1. What can be learned about the possible location of the interacting phosphate headgroup relative to the KcsA channel based on these distances? The following procedure was followed in determining the approximate position of the interacting ^{31}P nucleus. First, a sphere with radius 5 Å and origin centered on the nitrogen of the V48R1 nitroxide side chain was calculated. The interacting ^{31}P nucleus must be located on the surface of this sphere. Second, the surface area of the sphere in steric conflict with the channel was eliminated. Figure 5B shows the remaining phosphate interaction surface. Third, the possible interaction surface was further reduced by eliminating those areas that were >5 Å from any feasible R52R1 rotamer (Figure 5C). Fourth, the remaining surface was explored for steric compatibility with regard to a phosphate moiety. A phosphate group was moved along the surface, and all areas were eliminated where the phosphate is in steric conflict with the channel irrespective of its orientation. Finally, from this subset of sterically feasible phosphate

positions, we chose those that were within reach of the R52 side chain, assuming a native R52−phosphate interaction. The resulting set of possible phosphate positions is shown in Figure 5D (black models).

Several of these potential phosphate positions are highly compatible with the expected phosphate position based on a crystallographically determined lipid molecule. In the crystal structure of KcsA (PDB entries 1K4C and 1R3J), a lipid molecule binds to the channel in the groove between the inner helix of one subunit and the pore helix of the adjacent subunit. The lipid is resolved in two different orientations (green stick models in Figure 5D). Although the phosphate headgroup of this lipid could not be observed, the presence of the glycerol backbone in the model allows the possible locations of the nucleus to be determined (small yellow spheres). It is encouraging to note that several of the phosphate positions predicted by our placement are at a similar vertical position as the crystallographically predicted lipid phosphorus nucleus. In addition, the distance of closest approach between the crystallographically determined phosphorus nuclei positions and the modeled phosphate is on the order of ~8 Å and, thus, in reasonable agreement with the expected ~7 Å interphosphate distance in the membrane (*45*).

In this study, we have evaluated ESEEM in terms of its potential usefulness to describe the environment surrounding membrane proteins under native conditions. Using electron spin modulation by deuterium, we have demonstrated the water permeation profile along the surface of the KcsA potassium channel. The data support the conclusion that KcsA inserts into the membrane without creating water crevices along its protein surface. The technique may thus prove useful to detect the narrow water crevices that are predicted to occur in some membrane proteins as a result of distorted lipid packing (*48*, *49*). In addition, the ESEEM data identified two residues on KcsA through ^{31}P modulation that are in intimate contact with the phosphate headgroup region of the membrane. Based on a crystallographically determined structure of an interacting side chain, the position of the phosphate headgroup with respect to the channel could be strongly constrained. The data presented here demonstrate that the technique is well suited to investigate the interaction of membrane proteins with their surrounding lipid environment. This capability may prove particularly useful for the study of those proteins for which lipids are either critical for maintaining native structure or have been shown to participate in its function (*28*, *50*−*52*).

ACKNOWLEDGMENT

We thank Michael Lenaeus for critically reading the manuscript.

SUPPORTING INFORMATION AVAILABLE

A table with collection and refinement statistics of KcsA V48R1, a figure showing the unprocessed ESEEM data, a figure comparing the ^{2}H spectral density with collisional CW-EPR data, and additional crystallization and refinement methods. This material is available free of charge via the Internet at http://pubs.acs.org.

REFERENCES

1. Schweiger, A., and Jeschke, G. (2001) Principles of pulse electron paramagnetic resonance, 1st ed., Oxford University Press, Oxford.
2. Hoffman, B. M. (2003) Electron-nuclear double resonance spectroscopy (and electron spin-echo envelope modulation spectroscopy) in bioinorganic chemistry. *Proc. Natl. Acad. Sci. U.S.A. 100*, 3575–3578.
3. Mims, W. B., and Peisach, J. (1976) Assignment of a ligand in stellacyanin by a pulsed electron paramagnetic resonance method. *Biochemistry 15*, 3863–3869.
4. Prisner, T., Rohrer, M., and MacMillan, F. (2001) Pulsed EPR spectroscopy: biological applications. *Annu. Rev. Phys. Chem. 52*, 279–313.
5. Hoffman, B. M. (2003) ENDOR of metalloenzymes. *Acc. Chem. Res. 36*, 522–529.
6. Britt, R. D., Campbell, K. A., Peloquin, J. M., Gilchrist, M. L., Aznar, C. P., Dicus, M. M., Robblee, J., and Messinger, J. (2004) Recent pulsed EPR studies of the photosystem II oxygen-evolving complex: implications as to water oxidation mechanisms. *Biochim. Biophys. Acta 1655*, 158–171.
7. Erilov, D. A., Bartucci, R., Guzzi, R., Shubin, A. A., Maryasov, A. G., Marsh, D., Dzuba, S. A., and Sportelli, L. (2005) Water concentration profiles in membranes measured by ESEEM of spin-labeled lipids. *J. Phys. Chem. B 109*, 12003–12013.
8. Bartucci, R., Guzzi, R., Marsh, D., and Sportelli, L. (2003) Intramembrane polarity by electron spin echo spectroscopy of labeled lipids. *Biophys. J. 84*, 1025–1030.
9. Carmieli, R., Papo, N., Zimmermann, H., Potapov, A., Shai, Y., and Goldfarb, D. (2006) Utilizing ESEEM spectroscopy to locate the position of specific regions of membrane-active peptides within model membranes. *Biophys. J. 90*, 492–505.
10. Bartucci, R., Guzzi, R., Sportelli, L., and Marsh, D. (2009) Intramembrane water associated with TOAC spin-labeled alamethicin: electron spin-echo envelope modulation by D_2O. *Biophys. J. 96*, 997–1007.
11. Volkov, A., Dockter, C., Bund, T., Paulsen, H., and Jeschke, G. (2009) Pulsed EPR determination of water accessibility to spin-labeled amino acid residues in LHCIIb. *Biophys. J. 96*, 1124–1141.
12. Hubbell, W. L., Gross, A., Langen, R., and Lietzow, M. A. (1998) Recent advances in site-directed spin labeling of proteins. *Curr. Opin. Struct. Biol. 8*, 649–656.
13. Hubbell, W. L., Cafiso, D. S., and Altenbach, C. (2000) Identifying conformational changes with site-directed spin labeling. *Nat. Struct. Biol. 7*, 735–739.
14. Columbus, L., and Hubbell, W. L. (2002) A new spin on protein dynamics. *Trends Biochem. Sci. 27*, 288–295.
15. Fanucci, G. E., and Cafiso, D. S. (2006) Recent advances and applications of site-directed spin labeling. *Curr. Opin. Struct. Biol. 16*, 644–653.
16. Marsh, D. (2001) Polarity and permeation profiles in lipid membranes. *Proc. Natl. Acad. Sci. U.S.A. 98*, 7777–7782.
17. Marsh, D., Kurad, D., and Livshits, V. A. (2002) High-field electron spin resonance of spin labels in membranes. *Chem. Phys. Lipids 116*, 93–114.
18. Griffith, O. H., Dehlinger, P. J., and Van, S. P. (1974) Shape of the hydrophobic barrier of phospholipid bilayers. (Evidence for water penetration in biological membranes). *J. Membr. Biol. 15*, 159–192.
19. Altenbach, C., Greenhalgh, D. A., Khorana, H. G., and Hubbell, W. L. (1994) A collision gradient method to determine the immersion depth of nitroxides in lipid bilayers: application to spin-labeled mutants of bacteriorhodopsin. *Proc. Natl. Acad. Sci. U.S.A. 91*, 1667–1671.
20. Altenbach, C., Froncisz, W., Hemker, R., Mchaourab, H., and Hubbell, W. L. (2005) Accessibility of nitroxide side chains: absolute Heisenberg exchange rates from power saturation EPR. *Biophys. J. 89*, 2103–2112.
21. Schrempf, H., Schmidt, O., Kummerlen, R., Hinnah, S., Muller, D., Betzler, M., Steinkamp, T., and Wagner, R. (1995) A prokaryotic potassium ion channel with two predicted transmembrane segments from Streptomyces lividans. *EMBO J. 14*, 5170–5178.
22. Heginbotham, L., Kolmakova-Partensky, L., and Miller, C. (1998) Functional reconstitution of a prokaryotic K^+ channel. *J. Gen. Physiol. 111*, 741–749.
23. Zhou, Y., Morais-Cabral, J. H., Kaufman, A., and MacKinnon, R. (2001) Chemistry of ion coordination and hydration revealed by a K^+ channel-Fab complex at 2.0 Å resolution. *Nature 414*, 43–48.
24. le Coutre, J., Kaback, H. R., Patel, C. K., Heginbotham, L., and Miller, C. (1998) Fourier transform infrared spectroscopy reveals a rigid alpha-helical assembly for the tetrameric Streptomyces lividans K^+ channel. *Proc. Natl. Acad. Sci. U.S.A. 95*, 6114–6117.

25. Perozo, E., Cortes, D. M., and Cuello, L. G. (1998) Three-dimensional architecture and gating mechanism of a K^+ channel studied by EPR spectroscopy. *Nat. Struct. Biol. 5*, 459–469.
26. Gross, A., Columbus, L., Hideg, K., Altenbach, C., and Hubbell, W. L. (1999) Structure of the KcsA potassium channel from *Streptomyces lividans*: a site-directed spin labeling study of the second transmembrane segment. *Biochemistry 38*, 10324–10335.
27. Gross, A., and Hubbell, W. L. (2002) Identification of protein side chains near the membrane-aqueous interface: a site-directed spin labeling study of KcsA. *Biochemistry 41*, 1123–1128.
28. Vamvouka, M., Cieslak, J., Van Eps, N., Hubbell, W., and Gross, A. (2008) The structure of the lipid-embedded potassium channel voltage sensor determined by double-electron-electron resonance spectroscopy. *Protein Sci. 17*, 506–517.
29. Green, P. R., and Bell, R. M. (1984) Asymmetric reconstitution of homogeneous *Escherichia coli sn*-glycerol-3-phosphate acyltransferase into phospholipid vesicles. *J. Biol. Chem. 259*, 14688–14694.
30. Kumaresan, R., and Tufts, D. W. (1982) Estimating the parameters of exponentially damped sinusoids and pole-zero modeling in noise. *IEEE Trans. Acoust., Speech, Signal Process. 30*, 833–840.
31. Owenius, R., Osterlund, M., Svensson, M., Lindgren, M., Persson, E., Freskgard, P. O., and Carlsson, U. (2001) Spin and fluorescent probing of the binding interface between tissue factor and factor VIIa at multiple sites. *Biophys. J. 81*, 2357–2369.
32. Marsh, D., and Toniolo, C. (2008) Polarity dependence of EPR parameters for TOAC and MTSSL spin labels: correlation with DOXYL spin labels for membrane studies. *J. Magn. Reson. 190*, 211–221.
33. Kelly, B. L., and Gross, A. (2003) Potassium channel gating observed with site-directed mass tagging. *Nat. Struct. Biol. 10*, 280–284.
34. Cortes, D. M., Cuello, L. G., and Perozo, E. (2001) Molecular architecture of full-length KcsA: role of cytoplasmic domains in ion permeation and activation gating. *J. Gen. Physiol. 117*, 165–180.
35. Kurshev, V. V., and Kevan, L. (1995) Electron spin echo modulation studies of doxylstearic acid spin probes in frozen vesicle solutions: interaction of the spin probe with ^{31}P in the surfactant headgroups. *J. Phys. Chem. 99*, 10616–10620.
36. Hunte, C. (2005) Specific protein-lipid interactions in membrane proteins. *Biochem. Soc. Trans. 33*, 938–942.
37. Hofer, P., Grupp, A., Nebenfuhr, H., and Mehring, M. (1986) Hyperfine sublevel correlation (HYSCORE) spectroscopy - a 2D electron-spin-resonance investigation of the squaric acid radical. *Chem. Phys. Lett. 132*, 279–282.
38. Doyle, D. A., Cabral, J. M., Pfuetzner, R. A., Kuo, A., Gulbis, J. M., Cohen, S. L., Chait, B. T., and MacKinnon, R. (1998) The structure of the potassium channel: molecular basis of K^+ conduction and selectivity. *Science 280*, 69–77.
39. Tombolato, F., Ferrarini, A., and Freed, J. H. (2006) Dynamics of the nitroxide side chain in spin-labeled proteins. *J. Phys. Chem. B 110*, 26248–26259.
40. Oh, K. J., Altenbach, C., Collier, R. J., and Hubbell, W. L. (2000) Site-directed spin labeling of proteins. Applications to diphtheria toxin. *Methods Mol. Biol. 145*, 147–169.
41. Seelig, J., and Seelig, A. (1974) Deuterium magnetic resonance studies of phospholipid bilayers. *Biochem. Biophys. Res. Commun. 57*, 406–411.
42. Tugarinov, V., Kanelis, V., and Kay, L. E. (2006) Isotope labeling strategies for the study of high-molecular-weight proteins by solution NMR spectroscopy. *Nat. Protoc. 1*, 749–754.
43. Gordon-Grossman, M., Gofman, Y., Zimmermann, H., Frydman, V., Shai, Y., Ben-Tal, N., and Goldfarb, D. (2009) A combined pulse EPR and Monte Carlo simulation study provides molecular insight on peptide-membrane interactions. *J. Phys. Chem. B 113*, 12687–12695.
44. Noethig-Laslo, V., Cevc, P., Arcon, D., and Sentjurc, M. (2004) Hydrophobic barrier in liposomes studied by FT-ESEEM. *Origins Life Evol. Biosphere 34*, 237–242.
45. Engelman, D. M. (1971) Lipid bilayer structure in the membrane of *Mycoplasma laidlawii*. *J. Mol. Biol. 58*, 153–165.
46. Zanker, P. P., Jeschke, G., and Goldfarb, D. (2005) Distance measurements between paramagnetic centers and a planar object by matrix Mims electron nuclear double resonance. *J. Chem. Phys. 122*, 024515.
47. Halkides, C. J., Farrar, C. T., Larsen, R. G., Redfield, A. G., and Singel, D. J. (1994) Characterization of the active site of p21 ras by electron spin-echo envelope modulation spectroscopy with selective labeling: comparisons between GDP and GTP forms. *Biochemistry 33*, 4019–4035.
48. Freites, J. A., Tobias, D. J., von Heijne, G., and White, S. H. (2005) Interface connections of a transmembrane voltage sensor. *Proc. Natl. Acad. Sci. U.S.A. 102*, 15059–15064.
49. Freites, J. A., Tobias, D. J., and White, S. H. (2006) A voltage-sensor water pore. *Biophys. J. 91*, L90–L92.
50. MacKinnon, R. (2004) Structural biology. Voltage sensor meets lipid membrane. *Science 306*, 1304–1305.
51. Lee, S. Y., Lee, A., Chen, J., and MacKinnon, R. (2005) Structure of the KvAP voltage-dependent K^+ channel and its dependence on the lipid membrane. *Proc. Natl. Acad. Sci. U.S.A. 102*, 15441–15446.
52. Schmidt, D., Jiang, Q. X., and MacKinnon, R. (2006) Phospholipids and the origin of cationic gating charges in voltage sensors. *Nature 444*, 775–779.